




Correlations between polarization and structural information of supertetragonal PbTiO₃

Feng Zhang ^{1,2}, Jiale Zhang ^{1,2}, Hongmei Jing,³ Zhipeng Li,⁴ Dawei Wang ^{1,2,*} and Chun-Lin Jia^{1,5}

¹*School of Microelectronics and State Key Laboratory for Mechanical Behavior of Materials, Xi'an Jiaotong University, Xi'an 710049, China*

²*Key Lab of Micro-Nano Electronics and System Integration of Xi'an City, Xi'an Jiaotong University, Xi'an 710049, China*

³*School of Physics and Information Technology, Shaanxi Normal University, Xi'an 710062, China*

⁴*School of Materials Science and Engineering, University of Science and Technology Beijing, Beijing 100083, China*

⁵*Ernst Ruska Center for Microscopy and Spectroscopy with Electrons, Research Center Jülich, D-52425 Jülich, Germany*



(Received 9 November 2021; accepted 4 January 2022; published 13 January 2022)

The huge axial ratio of supertetragonal perovskites can induce large polarization due to the coupling between the unit cell and ion displacements, which often results in higher Curie temperature or better ferroelectric properties. With the progress of vertical strain engineering, experimentally available supertetragonal PbTiO₃ raises much interest in the relation between its intrinsic polarization and structural characteristics, such as the axial ratio and ion displacements that can be obtained with a high-resolution (scanning) transmission electron microscope nowadays. However, the interpretation and use of such obtained structural information are not without peril. Here, employing first-principles calculations, we report on the relationship between the polarization and the structural information for supertetragonal PbTiO₃. Our investigation shows that, unlike normal PbTiO₃, the strong sublinear correlation raises the difficulty to quantitatively estimate the spontaneous polarization for the axial ratio larger than 1.15. In addition, the relative displacement between cations (i.e., Pb and Ti) proves to be an unsuitable structural parameter to determine the spontaneous polarization, emphasizing the importance of obtaining the positions of anions, albeit presumably more difficult, along with cations.

DOI: [10.1103/PhysRevB.105.024106](https://doi.org/10.1103/PhysRevB.105.024106)

I. INTRODUCTION

Perovskites with the general formula ABO_3 have rich properties, such as ferroelectricity, piezoelectricity, superconductivity, and pyroelectricity, which can be employed in microelectromechanical systems, solar cells, and photodetectors [1–5]. Ferroelectric perovskites have played important roles in the fields of electronic transducers, pyroelectric sensors, film capacitors, actuators, nonlinear optical devices, and nonvolatile memories due to their excellent performance [6–12]. The intrinsic spontaneous polarization that arises from the displacement of ions, which is probably the most important feature of a ferroelectric perovskite, depends on its structural information, such as the axial ratio c/a and/or the off-center ion displacements, constituting a typical structure-property problem that requires both experimental and theoretical investigations [13–19].

While closely related, the polarization and structural information of a given system are usually obtained with different experimental setups; for instance, the electric hysteresis loop and x-ray diffraction (XRD) or high-resolution (scanning) transmission electron microscope [HR(S)TEM], respectively [20–26]. The link between the two rather independent experimental investigations, however, is not as strong as one may have expected. The standard empirical relation

$$P_S = \kappa \Delta z, \quad (1)$$

which is often used to predict the dipoles on each unit cell [23,24,27], was first derived from five displacive ferroelectrics in 1968 [28], not extensively examined afterwards with first-principles calculations.

In recent years, as aberration-corrected HR(S)TEM can accurately map ion displacements on the subatomic scale [29–32], the relation shown in Eq. (1) grows more important as it enables the direct estimation of the polarization from HR(S)TEM images. One advantage of this approach lies in its ability to extract the polarization induced by intrinsic effects (i.e., ion displacement and unit cell deformation), rather than that caused by extrinsic effects (e.g., space charge). Such a distinction can be crucial for many applications such as energy storage using ferroelectric materials [33,34]. However, for HR(S)TEM experiments, the application of Eq. (1) also involves an interesting subtlety; that is, how to determine Δz from HR(S)TEM images. For the perovskite ABO_3 , there are at least two choices: (i) Δz is defined as the displacement of the B atom relative to the center of its eight neighboring A -site atoms [35] [usually only four can be seen in a HR(S)TEM image]; (ii) Δz is defined as the displacement of the B atom relative to its enclosing oxygen octahedron [23,24,27]. The first choice is popular since all the cations can be seen under the high angle annular dark field (HAADF) imaging condition (see Sec. II B). The second choice requires techniques, such as negative spherical-aberration (Cs) imaging (NCSI) [29] and annular bright field (ABF) imaging [36], to see the anions (i.e., oxygens for PbTiO₃). We find that first-principles calculations can help understand which one is a better choice. While the relative displacements between cations provide important

*dawei.wang@xjtu.edu.cn

structural information, our investigation shows that imaging anions is also critical to quantitatively predict the dipoles on each unit cell and, consequently, the macroscopic polarization, for supertetragonal perovskites.

Also in recent years, vertical strain engineering via interfacial coupling between different components has emerged as an important perovskite growth technique. Vertically aligned and strained systems have been developed [37,38] and supertetragonal PbTiO_3 was observed [27,39,40]. Such experimental progress with supertetragonal perovskites casts some doubt on Eq. (1) as the linear relation may be invalidated for the huge axial ratio, where the correlation between spontaneous polarization and the structural information needs further investigation.

It is clear that addressing the aforementioned problems will help better utilize HR(S)TEM images to predict the properties of ferroelectric perovskites. To resolve these issues adequately, we hope to achieve three goals in this work. First, we will examine and establish the relation between spontaneous polarization and structural information, which includes both the axial ratio and ion displacements. We will focus on PbTiO_3 since vertical strain engineering has been realized for it [27,39,40], therefore, the huge axial ratio requires a revisit of the linear relation assumption as shown in Eq. (1). Second, we will clarify how the ion displacement Δz shall be defined and used. With HAADF images, the relative displacements between cations can be obtained [35,39]. For PbTiO_3 it is

$$P_S = \kappa \Delta_{\text{Ti-Pb}}, \quad (2)$$

where $\Delta_{\text{Ti-Pb}}$ is the Ti shift with respect to the center of the enclosing Pb atoms. On the other hand, an alternative link between the spontaneous polarization and the off-center ion displacements is given by [28]

$$P_S = \kappa \Delta_{\text{Ti-O}}, \quad (3)$$

where $\Delta_{\text{Ti-O}}$ is the Ti atom off-center displacements with respect to O atoms, and κ equals to $2580 (\mu\text{C}/\text{cm}^2)/\text{nm}$ for PbTiO_3 . This is also the formula used to estimate the polarization from aberration-corrected HR(S)TEM images [27]. We will investigate the subtle difference between these two formulas. Third, we will compare first-principles calculation results to available experimental findings in order to establish quantitative relations between the polarization and the axial ratio [16,17] as well as the displacements $\Delta_{\text{Ti-O}}$ and $\Delta_{\text{Ti-Pb}}$ [28], in particular, extending the strain range to cover supertetragonal PbTiO_3 . Moreover, since the PbTiO_3 under huge vertical strain will break and become a layered structure at some point, the axial ratio cannot increase the polarization of PbTiO_3 indefinitely. Our first-principles calculations will find how large the intrinsic polarization can be for PbTiO_3 at a given epitaxial strain.

This paper is organized as follows. In Sec. II, we will discuss the fabrication, HR(S)TEM imaging, and first-principles calculations of supertetragonal PbTiO_3 . In particular, we will discuss the details of the first-principles calculations in this section. In Sec. III, we will show the first-principles calculation results concerning the correlation between the spontaneous polarization and various structural information, and discuss their implications. Finally, in Sec. IV, we provide a brief conclusion.

II. METHODS

As a typical ferroelectric material, PbTiO_3 has excellent properties including high Curie temperature, high thermoelectric coefficient, and large polarization ($\sim 75 \mu\text{C}/\text{cm}^2$) [41,42]. Surpassing the large tetragonality of bulk PbTiO_3 ($c/a \simeq 1.06$) [43], supertetragonal PbTiO_3 with even larger c/a was achieved in recent years. In this section, we will discuss three aspects relating to the fabrication, HR(S)TEM imaging, and first-principles calculation of supertetragonal PbTiO_3 .

A. Fabrication

Supertetragonal PbTiO_3 (PTO) with large c/a was first reported to exist in PTO-PbO nanocomposite thin films, which were epitaxially grown on LaAlO_3 substrate [44,45]. In 2018, Zhang *et al.* [39] proposed a new “phase-to-phase strain” strategy and achieved huge polarization on the ultratetragonal film. Using two materials with similar lattice structure, different lattice parameters are matched on the grain boundary during the epitaxial growth using simple radio-frequency magnetron sputtering, generating isotropic strains between the materials and introducing high negative pressure on PbTiO_3 to achieve huge polarization. The lattice parameters of the thin films ($a = 0.3923 \text{ nm}$, $c = 0.4857 \text{ nm}$) were measured by XRD and x-ray reciprocal space mappings.

In a more recent experimental work [40], a pulsed laser deposition system was used to grow an epitaxial film with two layers of $\text{PbTiO}_3/\text{LaSrMnO}_3$ on a (001) oriented SrTiO_3 substrate. The self-assembled nanocomposite film contains nanoscale PbTiO_3 columnar grains surrounded by the matrix of the PbO structure. The structural parameters, crystalline quality, and orientation relationship of the multilayer films were characterized by high-resolution XRD with all the layers showing a cubic-on-cubic relationship with the SrTiO_3 substrate. In a related work, the NCSI technique provides more structural information of the vertically strained PbTiO_3 [27], where the measured a - and c -lattice constants of the PbTiO_3 film are 0.384 and 0.469 nm, respectively, resulting in a $c/a = 1.221$. It is also found that the average off-center displacement of Ti relative to the O atoms is 0.052 nm.

B. HR(S)TEM

In practice, several HR(S)TEM techniques can be used to investigate the dipole/polarization in a supertetragonal PbTiO_3 . For instance, the HAADF technique can be used directly to image cations. Under the HAADF imaging conditions, the atomic column intensity is approximately proportional to Z^2 , where Z is the atomic number averaged along the atom columns [46]. Therefore, HAADF is also called Z -contrast image, which can be used to distinguish different elements [47–50]. The Z -contrast image changes slowly and smoothly with the specimen thickness and the defocus of the objective lens [51]. Unfortunately, oxygen columns in PTO cannot be imaged under HAADF imaging conditions due to the fact that the Z of the oxygen atom is too low in comparison to the surrounding Pb atoms. On the other hand, the ABF technique can work as an imaging mode to supplement HAADF with its ability to image light elements such as oxygen, nitrogen, and lithium [36].

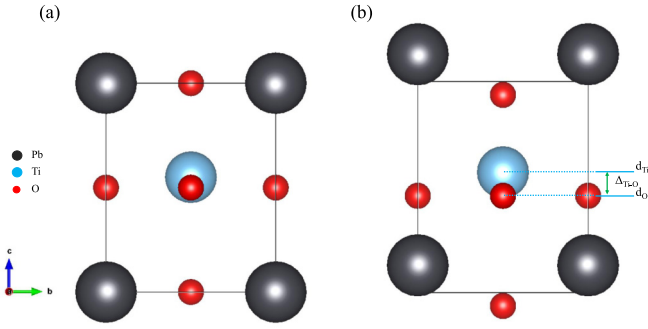


FIG. 1. The structure of PbTiO_3 with the lattice parameters $a = b = 0.385$ nm and $c = 0.475$ nm. (a) The initial tetragonal phase structures have different c -axis lattice constants. (b) After relaxation, the displacement between the center Ti and the surrounding oxygen atoms can be clearly seen.

For the thin specimen, using the NCSI technique, all atomic positions are visible (including oxygen) and the position of each atom can be measured sensitively with the precision of picometers [52,53]. The powerful NCSI technique has enabled the studies of atomic displacements, defects, and surface structures. Therefore, in principle, for PbTiO_3 , HAADF can provide $\Delta_{\text{Ti-Pb}}$ and c/a , while NCSI and ABF can provide the extra $\Delta_{\text{Ti-O}}$. After that, the dipoles on each unit cell or the macroscopic spontaneous polarization P_S can be calculated using the measured atomic shifts, employing the effective charges of the ions [54] or the empirical relation in Eq. (1).

C. First-principles calculation

The opportunity with supertetragonal PbTiO_3 has attracted much attention in the hope to achieve super properties, such as a super large polarization [55–57]. From a theoretical point of view, it is important to know how the polarization is correlated with structural information, including the tetragonality and the off-center displacements, which can be extracted from HR(S)TEM images. For instance, using Eq. (3), the polarization for $\Delta_{\text{Ti-O}} = 0.052$ nm and $\kappa = 2580$ ($\mu\text{C}/\text{cm}^2$)/nm is estimated to be 134 $\mu\text{C}/\text{cm}^2$ [27]. First-principles calculation will help determine if the linear dependence of the polarization on the ionic displacements fails at huge c/a [28]. In the past, first-principles calculations have focused on the low to medium c/a values, mostly around 1.06, in order to compare with experimental results [58,59]. As strain engineering can tune the properties of PbTiO_3 [60], it was found that when the average c/a increases ($c/a \simeq 1.09, 1.10, 1.11$), the calculated spontaneous polarization increases as well (the values are 80, 90, and 100 $\mu\text{C}/\text{cm}^2$) [61,62]. In this work, in the first-principles calculations, we choose the in-plane lattice constant of PbTiO_3 to be 0.385 nm to mimic the in-plane constraint, and change the c axis from 0.385 to 0.560 nm to explore the effects of the vertical strain [61,62].

The strained PbTiO_3 is then relaxed to optimize the ion positions. Figure 1 shows one of the structures used in our calculations, which has an axial ratio $c/a = 1.234$. Figure 1(a) shows the initial setup of the tetragonal phase PbTiO_3 with the lattice parameters $a = b = 0.385$ nm and $c = 0.475$ nm

and Fig. 1(b) shows the structure after the relaxation of ion positions. From first-principles calculations, we can obtain $\Delta_{\text{Ti-O}} = |d_{\text{Ti}} - \bar{d}_{\text{O}}|$ or $\Delta_{\text{Ti-Pb}} = |d_{\text{Ti}} - \bar{d}_{\text{Pb}}|$ using the optimized ion positions where d_{Ti} represents the displacement of the Ti atom along the c axis, and \bar{d}_{O} (\bar{d}_{Pb}) represents the average displacement of the enclosing O (Pb) atoms along the c axis. In aberration-corrected HR(S)TEM images, $\Delta_{\text{Ti-O}}$ and $\Delta_{\text{Ti-Pb}}$ can be determined by measuring the positions of the intensity peaks corresponding to the atomic columns.

The first-principles calculations are carried out using GPAW [63] and ABINIT [64] with the Perdew-Burke-Ernzerhof (PBE) exchange-correlation functional [65]. An energy cutoff of 750 eV and a $4 \times 4 \times 4$ mesh for the Brillouin-zone integration are used to ensure the convergence. Structural relaxations are performed until all the forces on the atoms are less than 0.005 eV/Å. The polarization of each relaxed configuration is obtained with the Berry phase approach [66]. As an alternative, using GPAW, we have also obtained the Born effective charge (BEC), which is then used to calculate the polarization along the c axis with the formula [67]

$$P_S = P_z = \frac{1}{V} \sum_i Z_{i,z}^* \mu_{i,z}, \quad (4)$$

where spontaneous polarization (P_S) is along the c axis (P_z). In the above equation, V is the volume of the unit cell, Z_i^* is the BEC, and μ_i refers to the displacement of the ion i (i is the index of ions in one unit cell).

III. RESULTS AND DISCUSSION

When the positions of Pb and Ti are determined from aberration-corrected HR(S)TEM images, the axial ratio and $\Delta_{\text{Ti-Pb}}$ can be determined. The ABF or NCSI can also see the positions of oxygen atoms, therefore determining $\Delta_{\text{Ti-O}}$. As a HR(S)TEM experiment can obtain the dipoles on each unit cell, it provides information about large-scale dipole patterns, such as domains and domain boundaries [24,68], or the macroscopic polarization. In order to quantitatively determine the dipole or the polarization, it is necessary to employ first-principles calculation to understand how the axial ratio and $\Delta_{\text{Ti-O}}$ ($\Delta_{\text{Ti-Pb}}$) are connected to the polarization. Moreover, we will also discuss the relation between $\Delta_{\text{Ti-O}}$ and $\Delta_{\text{Ti-Pb}}$ to emphasize the importance of obtaining the oxygen positions from HR(S)TEM images.

A. c/a

We first check how the polarization and the relative ion displacement between Ti and O ($\Delta_{\text{Ti-O}}$) depend on the axial ratio c/a . Figure 2(a) shows the polarization of the PbTiO_3 as a function of the axial ratio while the in-plane lattice constant is fixed to $a = 0.385$ nm. There are three lines in this plot: (i) The purple dotted line with circles is directly calculated with GPAW; (ii) the blue dotted line with triangles is obtained with ABINIT; and (iii) the green dotted line with diamonds is obtained using the BEC and ion displacements (see below). The first two results are obtained with the Berry phase approach while the third one needs to calculate the BEC first. The third one shows slightly larger values when $c/a > 1.2$, which is less accurate since the BECs relate to the first order derivative

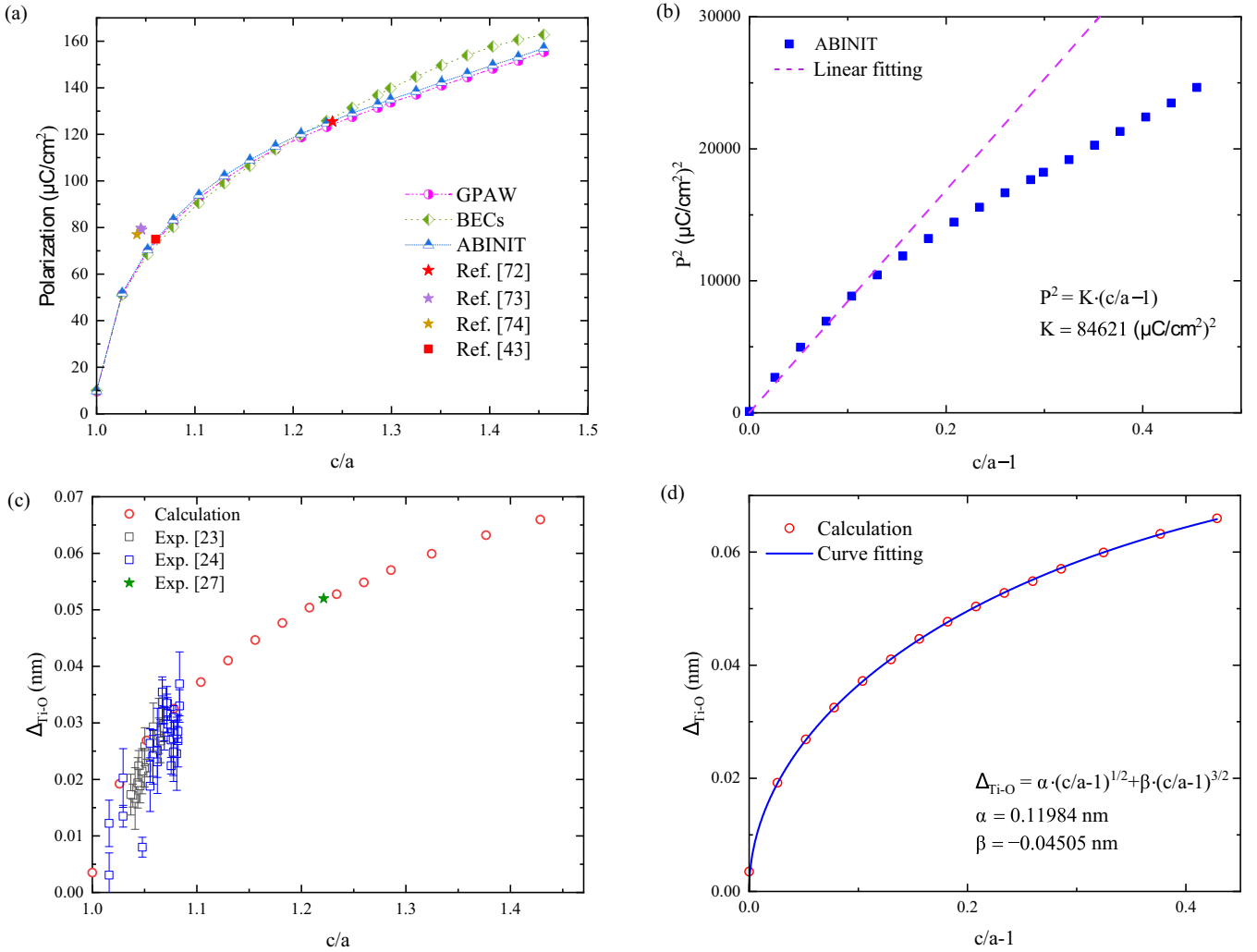


FIG. 2. (a) The relationship between the polarization of PbTiO₃ versus the axial ratio c/a shows a strong nonlinear feature. The purple dotted line is directly calculated with GPAW; the green dotted line is obtained by first calculating the BEC with GPAW, and then using Eq. (4) to calculate the polarization; the blue dotted line represents the polarization calculated with ABINIT. Other known values from literature, including the value for the bulk, are also shown in this plot as symbols. (b) The relationship between polarization and $c/a - 1$ of PbTiO₃. (c) The relationship between off-center displacement of Ti atoms in PbTiO₃ and Pb(Zr, Ti)O₃ structures and c/a . The data indicated by blue with error bars [23,24] and a green star [27] are from experiments. The red circle is obtained through the optimized structure by GPAW. (d) Curve fitting of the correlation between the relative displacement of Ti-O and $c/a - 1$.

of the P_3 -versus-displacement curves [69–71]. In general, the three sets of results agree very well. Figure 2(a) also contains four scattered points that are from the literature with details shown in Table I, which have used either PBE [43,72] or local density approximation (LDA) [73,74]. The overall agreement between our results and the others is very good. In addition,

TABLE I. Calculation results of PbTiO₃ in different works.

References	c/a	Polarization ($\mu\text{C}/\text{cm}^2$)
VASP [72]	1.240	125.5
VASP (LDA) [73]	1.046	79
PWSCF [74]	1.041	77
Bulk PbTiO ₃ [43]	1.06	75

Fig. 2(a) also shows that the dependence of the polarization on c/a is strongly nonlinear.

From the Landau-Ginzburg-Devonshire (LGD) theory [13,40,75–77], it is known that P^2 is linearly dependent on c/a . However, Fig. 2(b) shows that, for PbTiO₃, the linear dependence is no longer valid when $c/a \gtrsim 1.15$. In this plot, the blue squares are obtained using ABINIT and the purple dotted line represents a linear fitting for the region of the small axial ratio. We can see that the polarization for $c/a < 1.15$, P^2 is indeed proportional to the c/a as $P^2 \simeq K(c/a - 1)$ [16] where $K = 84621 (\mu\text{C}/\text{cm}^2)^2$. This linear relation between P^2 and c/a eventually breaks down at large c/a , making it more difficult to directly predict the polarization from the axial ratio.

Since a HR(S)TEM image reveals many slightly different unit cells, it can be used to map the axial ratio to the ion displacement for each unit cell, therefore providing a

statistical relation for the two variables. Figure 2(c) compares experimentally obtained [23,24,27] $\Delta_{\text{Ti-O}}$ versus c/a to first-principles calculation results. Most of the experimental results are around the axial ratio of bulk PbTiO_3 ($c/a < 1.1$) with one exception [27]. The experimental values and first-principles calculation results are superimposed on Fig. 2(c), which clearly shows their consistency over the whole range of c/a . For the supertetragonal case (indicated by the green star), $c/a \simeq 1.22$ ($c = 0.469$ nm), it was found that $\Delta_{\text{Ti-O}} = 0.0516$ nm from first-principles calculations, agreeing quite well with the corresponding experimental value (0.052 nm) [27]. It can be seen that $\Delta_{\text{Ti-O}}$ is not linearly dependent on c/a either. In fact, the dependence can be fitted by

$$\Delta_{\text{Ti-O}} = \alpha \left(\frac{c}{a} - 1 \right)^{1/2} + \beta \left(\frac{c}{a} - 1 \right)^{3/2}, \quad (5)$$

as shown in Fig. 2(d), where $\alpha = 0.11984$ nm, $\beta = -0.04505$ nm. In addition to the direct Berry phase method [66], in order to estimate the dipoles on each unit cell, one can multiply the ion displacements by the BEC, which is the first order derivative of polarization with respect to ion displacement. Figure 3 shows how these two quantities, both of which are obtained with GPAW, evolve with the axial ratio.

Figure 3(a) shows that the BECs decrease in magnitude with the increasing axial ratio. In particular, the effective charge Z_{Ti}^* changes from ~ 7 to ~ 4 when c/a increases from 1 to 1.45. This change likely arises as the charge transfer between anions and cations becomes smaller when the ions get farther away from each other. A comprehensive discussion on BECs can be found in Ref. [78] and similar trends have also been reported in PbTiO_3 films and superlattices under small strains [79,80].

Figure 3(b) shows that the ion displacements increase with c/a and the cations (Pb and Ti) shift in the opposite direction to the anions (O). More importantly, this plot also indicates that $\Delta_{\text{Ti-O}}$ and $\Delta_{\text{Ti-Pb}}$ have opposite signs, which shall be heeded when $\Delta_{\text{Ti-Pb}}$ is used to find the direction of dipoles in a HR(S)TEM image. This is a tricky issue because, for instance, $\Delta_{\text{Ti-O}}$ and $\Delta_{\text{Ti-Ba}}$ have the same sign for BaTiO_3 [81], unlike PbTiO_3 . We note that the ferroelectric polarization had also been estimated using a more complex formula from the LGD theory [40,76,77],

$$P_s = \left[\frac{x_s - 2s_{12}x_m/(s_{11} + s_{12})}{Q_{11} - 2s_{12}Q_{12}(s_{11} + s_{12})} \right]^{1/2}, \quad (6)$$

where a and c are the in-plane and out-of-plane lattice constant, respectively, a_p is the lattice constant of the paraelectric cubic phase extrapolated to room temperature [82], $x_s = (c - a_p)/a_p$, and $x_m = (a - a_p)/a_p$. In addition, s_{ij} is the elastic compliance and Q_{ij} is the electrostrictive coefficient. The values of these parameters for PbTiO_3 can be found in Ref. [83]. Substituting different c values into the above equation, we find the corresponding P_s , shown in Fig. 4, indicating that, except around the c/a of bulk PbTiO_3 (~ 1.06), Eq. (6) overestimates the polarization by a large margin.

B. $\Delta_{\text{Ti-O}}$ and $\Delta_{\text{Ti-Pb}}$

While the axial ratio can be obtained from HR(S)TEM images, the results in Sec. III A indicate that it does not pro-

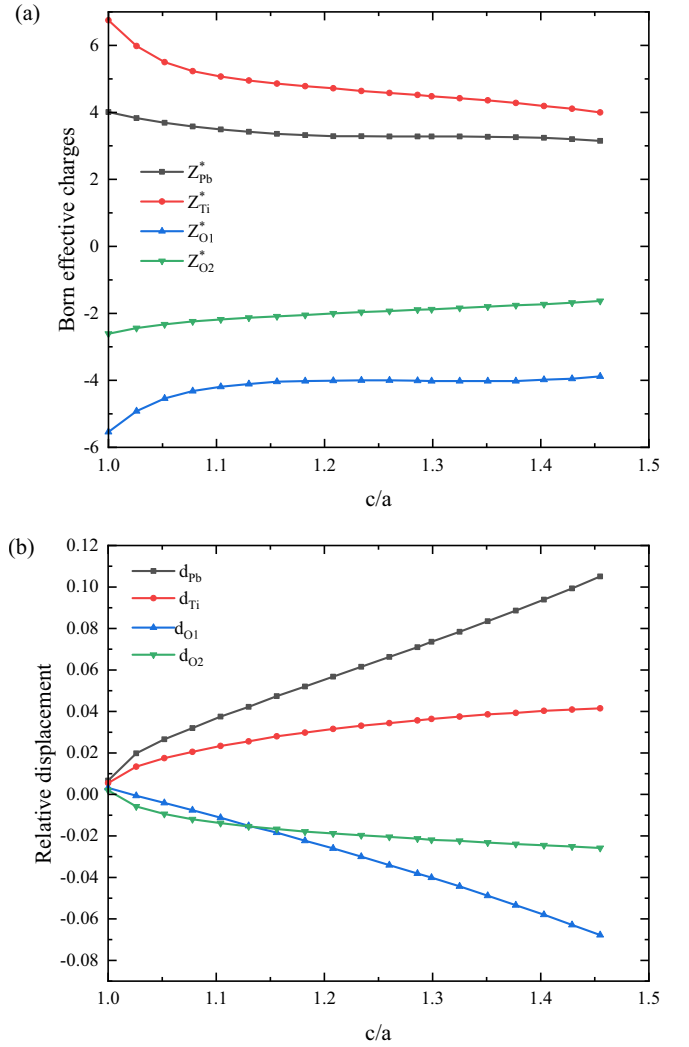


FIG. 3. (a) BECs and (b) relative displacement of each atom of PbTiO_3 under different c/a . Here, O_1 refers to the two O ions at the upper and lower vertices of the oxygen octahedron and O_2 refers to the other four O ions.

vide the best structural information to quantitatively predict the polarization and a linear relation will be preferred. As discussed in Sec. II B, under the NCSI imaging condition, the relative displacement between the B site atoms and the surrounding oxygen octahedron ($\Delta_{\text{Ti-O}}$) can also be obtained in addition to c/a and $\Delta_{\text{Ti-Pb}}$. In this section, we examine the relation between the polarization and $\Delta_{\text{Ti-O}}/\Delta_{\text{Ti-Pb}}$.

The linear increase of the polarization with $\Delta_{\text{Ti-O}}$, as shown in Fig. 5, stops at $P \simeq 100 \mu\text{C}/\text{cm}^2$ (or $c/a \simeq 1.13$) when it becomes sublinear. The fitting of the linear part agrees very well with the empirical formula $P_s = \kappa \Delta_{\text{Ti-O}}$ with the slope $\kappa = 2580 (\mu\text{C}/\text{cm}^2)/\text{nm}$ close to the originally reported value $(2510 \pm 70) (\mu\text{C}/\text{cm}^2)/\text{nm}$ [28]. This result explains why $\Delta_{\text{Ti-O}}$ (or $\Delta_{\text{Fe-O}}$) has been often used to estimate dipoles in $\text{Pb}(\text{Zr}, \text{Ti})\text{O}_3$ and BiFeO_3 [23,24,53,84].

From HAADF images, $\Delta_{\text{Ti-Pb}}$ can also be obtained and used as an alternative to $\Delta_{\text{Ti-O}}$. Therefore, it is beneficial to examine how the polarization changes with it. Figure 6(a) shows the polarization as a function of $\Delta_{\text{Ti-Pb}}$, where the negative

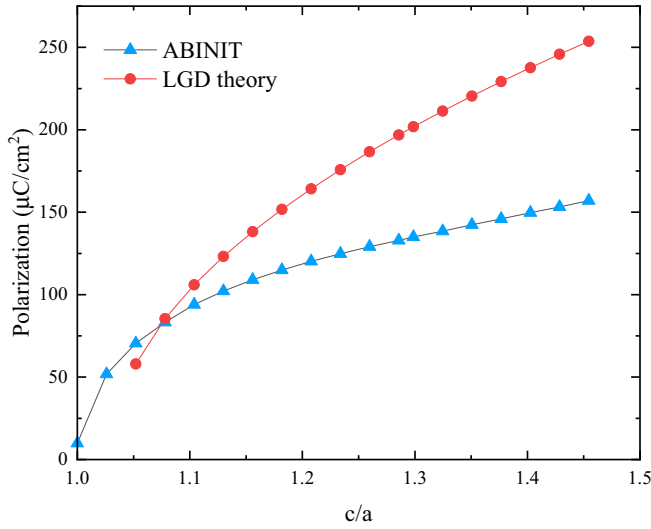


FIG. 4. The relationship between polarization calculated based on LGD theory and c/a . The red dot is the value calculated by the LGD theory, and the blue triangle is the polarization calculated by ABINIT.

polarization indicates that it is opposite to $\Delta_{\text{Ti-Pb}}$. Since the overall dependence of the polarization on $\Delta_{\text{Ti-Pb}}$ is highly non-linear, the polarization of the supertetragonal PbTiO_3 cannot be accurately obtained by comparing the $\Delta_{\text{Ti-Pb}}$ in the supertetragonal phase to its bulk value ($\Delta_{\text{Ti-Pb}} = 0.01$ nm, consistent with Ref. [85]) and assuming a linear relation. Figure 6(b) compares $\Delta_{\text{Ti-Pb}}$ to $\Delta_{\text{Ti-O}}$, again showing a strong nonlinear relation. The negative value of $\Delta_{\text{Ti-Pb}}$ also indicates that it is opposite to $\Delta_{\text{Ti-O}}$.

The above results demonstrate that $\Delta_{\text{Ti-Pb}}$ and $\Delta_{\text{Ti-O}}$ are very different quantities. While P_S is almost linearly dependent on $\Delta_{\text{Ti-O}}$ over the whole range (see Fig. 5), P_S 's

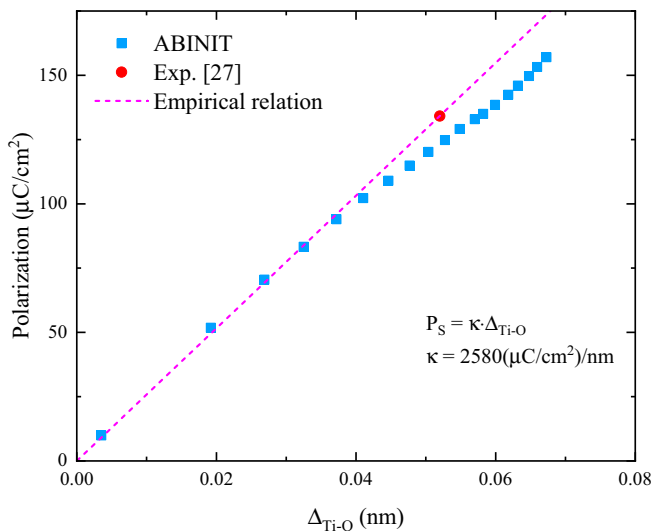


FIG. 5. The relationship between polarization and $\Delta_{\text{Ti-O}}$ of PbTiO_3 . The purple dotted line represents the empirical relation, the blue squares are calculated values, and the red dot is the estimated value [using the empirical relation Eq. (3)] obtained in the experiment [27].

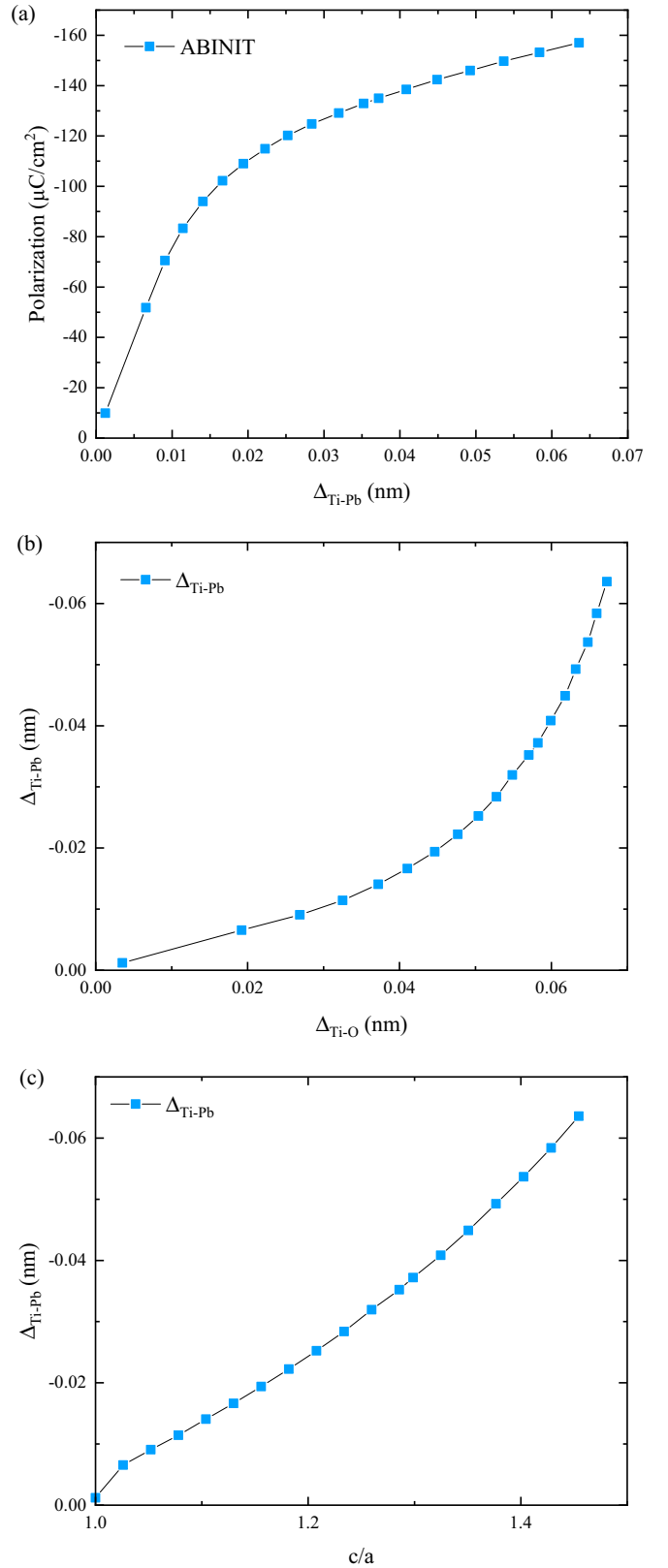


FIG. 6. (a) The relationship between polarization and $\Delta_{\text{Ti-Pb}}$. (b) The relationship between $\Delta_{\text{Ti-Pb}}$ and $\Delta_{\text{Ti-O}}$. (c) The relationship between $\Delta_{\text{Ti-Pb}}$ and c/a .

increase with $\Delta_{\text{Ti-Pb}}$ slows down significantly when $\Delta_{\text{Ti-Pb}}$ is large [see Fig. 6(a)]. Moreover, Fig. 6(c) shows a mostly linear

correlation between $\Delta_{\text{Ti-Pb}}$ and c/a , indicating that $\Delta_{\text{Ti-Pb}}$ is more like the axial ratio rather than $\Delta_{\text{Ti-O}}$ in terms of the structural information it provides.

C. Discussion

The results in Secs. III A and III B show that the polarization depends nonlinearly on c/a , $\Delta_{\text{Ti-Pb}}$, and $\Delta_{\text{Ti-O}}$ for supertetragonal PbTiO_3 . In addition, for small c/a , P^2 (instead of P) is proportional to $c/a - 1$ for $c/a \lesssim 1.15$ [see Fig. 2(b)], which was first considered by Devonshire [13]. The well known Landau-Devonshire theory constructs a free energy that includes the coupling between polarization and strain, $P^2\eta$, where η is the vertical strain [13,75]. The absence of the linear coupling $P\eta$ due to symmetry arguments leads to a linear correlation between P^2 and η (or c/a) for small tetragonality. The interplay between the tetragonality, ion displacements, and polarization has also been investigated later [18].

For small tetragonality, we have so far found three linear relations: (i) P^2 linearly depends on c/a [see Fig. 2(b)]; (ii) P linearly depends on $\Delta_{\text{Ti-Pb}}$ [see Fig. 6(a)]; and (iii) P linearly depends on $\Delta_{\text{Ti-O}}$ (see Fig. 5). However, only the last one can be extended to large tetragonality without introducing too much error. In fact, for very large tetragonality ($c/a \geq 1.15$), these three linear relations are all violated.

Our results indicate that the polarization for supertetragonal PbTiO_3 cannot be estimated from c/a or $\Delta_{\text{Ti-Pb}}$ by assuming a linear dependence. Moreover, the eventual breakdown of the linear relation between the polarization and $\Delta_{\text{Ti-O}}$ is not surprising since $\Delta_{\text{Ti-O}}$ alone cannot account for the other factors, such as the displacement of Pb, that can also affect the polarization. In fact, the robustness of this linear relation up to $c/a = 1.15$ is surprising since the bulk PbTiO_3 only has a $c/a \simeq 1.06$. The relation between polarization and $\Delta_{\text{Ti-O}}$ can be improved by examining how the BECs change with $\Delta_{\text{Ti-O}}$. Figure 7(a) shows that Z_i^* (where i can be Pb, Ti, or O) has an approximate linear dependence on $\Delta_{\text{Ti-O}}$, i.e.,

$$Z_i^* = Z_i^{0*} + \alpha_i \Delta_{\text{Ti-O}}, \quad (7)$$

where α_i is a coefficient depending on the ion type i . The change of BECs should not come as a surprise because, as ion displacements increase from their equilibrium positions (i.e., the bulk state with smaller tetragonality), the ionic bonding becomes weaker, implying less charge transfer between cations to anions. In addition, previous investigation [81] indicates that the ion displacements in PbTiO_3 are linearly correlated with respect to P (or equivalently to $\Delta_{\text{Ti-O}}$ as a first order approximation according to Fig. 5), i.e.,

$$d_i = \beta_i \Delta_{\text{Ti-O}}. \quad (8)$$

Combining the above two equations, we found that

$$P_S = \sum_i Z_i^* d_i = A \Delta_{\text{Ti-O}} + B (\Delta_{\text{Ti-O}})^2, \quad (9)$$

where $A = \sum_i Z_i^{0*} \beta_i$ and $B = \sum_i \alpha_i \beta_i$, which explains why the polarization linearly depends on $\Delta_{\text{Ti-O}}$ when its value is small, but deviation occurs at large $\Delta_{\text{Ti-O}}$. This quadratic equation can fit the P_S -versus- $\Delta_{\text{Ti-O}}$ curve very well over the whole range as shown in Fig. 7(b). Given the analysis on ion displacements [81], we may conclude that the above relation is quite general, valid for many ferroelectric and dielectric ma-

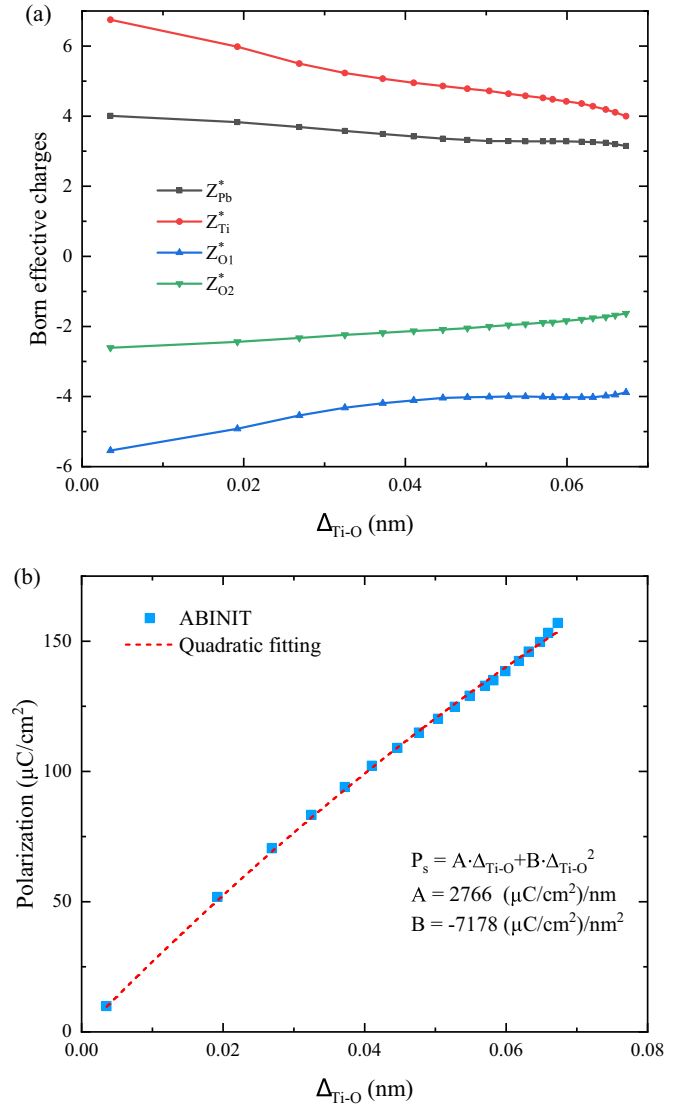


FIG. 7. (a) The relationship between BECs and $\Delta_{\text{Ti-O}}$. (b) The formula fitting for polarization and $\Delta_{\text{Ti-O}}$ of PbTiO_3 .

terials, including BaTiO_3 , PbTiO_3 , and BaZrO_3 . It constitutes a useful relation for the analysis of HR(S)TEM images using relative displacement to predict the polarization.

From Fig. 6, we see that $\Delta_{\text{Ti-Pb}}$ is not an ideal parameter to estimate the polarization. Strictly speaking, polarization arises from the separation between cations and anions; the relative displacement between cations (e.g., $\Delta_{\text{Ti-Pb}}$) does not represent the polarization well. Moreover, as Pb has more room for displacement than Ti (since Pb is between oxygen octahedra while Ti is inside the octahedron), it can displace much more than Ti with increasing c/a as evidenced by Fig. 3(b), resulting in a closer relation between $\Delta_{\text{Ti-Pb}}$ and c/a (instead of polarization) as shown in Fig. 6(c). Finally, let us find the maximum intrinsic polarization of a supertetragonal PbTiO_3 when its in-plane lattice constant is fixed (0.385 nm) and the out-of-plane lattice constant stretched. Clearly, the polarization in PbTiO_3 cannot increase with c/a indefinitely because, at some point, the ions will be separated so far away that no charge transfer occurs, resulting in null polarization.

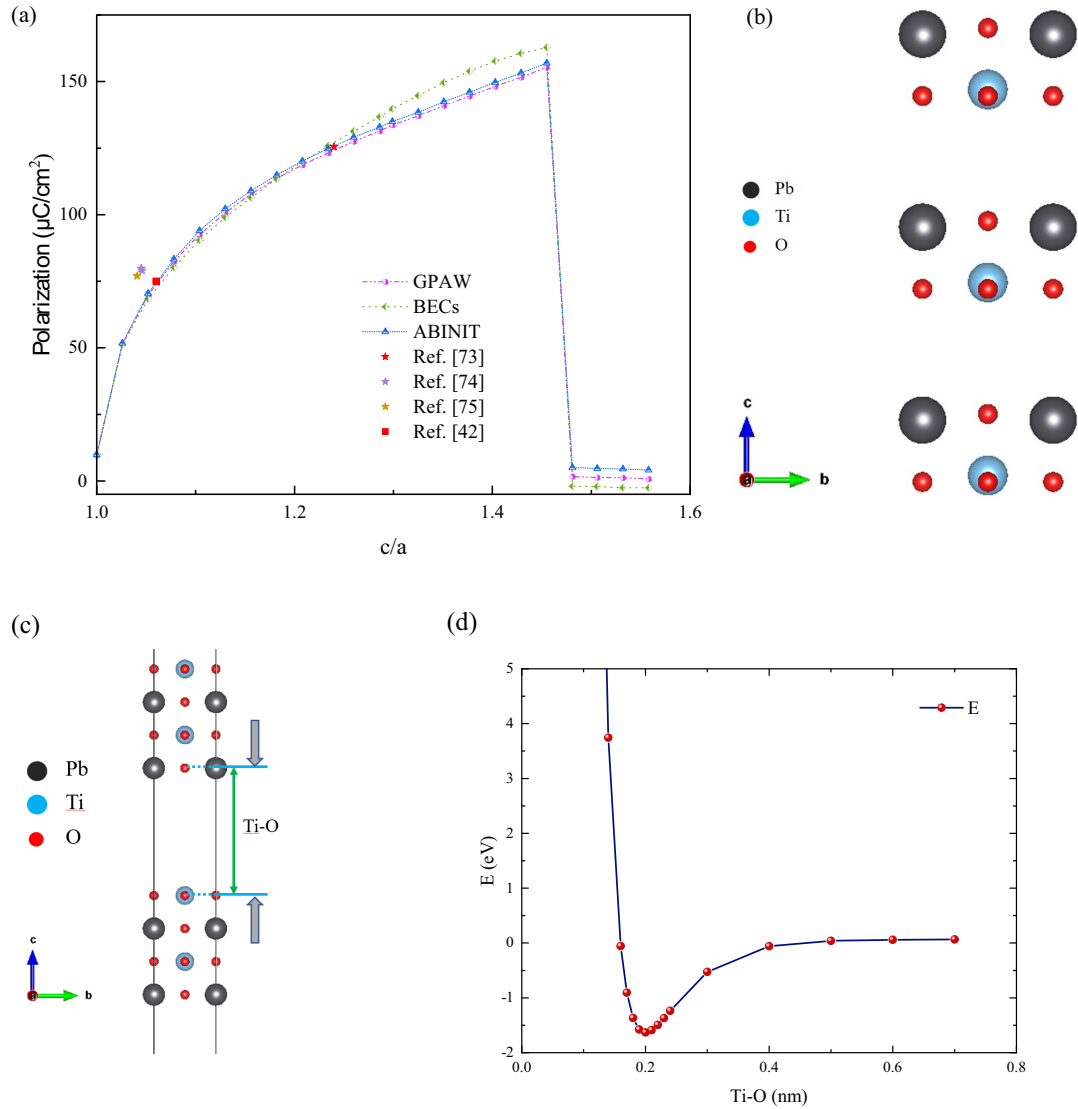


FIG. 8. (a) The relationship between the polarization of PbTiO_3 versus the axial ratio c/a . (b) The layered structure of PbTiO_3 when $c/a > 1.455$. (c) The structure obtained by cutting the bulk PbTiO_3 into two parts with a PbO surface and a TiO surface; the distance of Ti-O is shown by the green arrow in the figure. (d) The relationship between energy change and Ti-O distance.

To this end, we continue the first-principles calculation of the polarization until $c/a = 1.558$ with the results shown in Fig. 8(a). We find that the relaxed PbTiO_3 will break down into layered structures at $c/a \approx 1.455$ (or the c -axis lattice constant is at 0.56 nm) as shown in Fig. 8(b). As the delamination of the PbTiO_3 appears, the polarization of this system suddenly goes to zero. Therefore, the intrinsic polarization reaches the maximum value of $P_S \approx 155 \mu\text{C}/\text{cm}^2$. Larger polarization observed in an experiment may come from other contributions.

When the delamination occurs, the distance between the separated layers is 0.39 nm as shown in Fig. 8(b). To verify this result, we also obtain the interface bonding energy by cutting the PbTiO_3 into two parts [see Fig. 8(c)] and varying the distance between them (without structure relaxation). The interface bonding energy is calculated with $E = E_{\text{tot}} - E_{\text{part-1}} - E_{\text{part-2}}$ where E_{tot} represents the total energy of the entire structure and $E_{\text{part-1}}$ ($E_{\text{part-2}}$) represents the energy of

the upper (lower) half of the structure. Figure 8(d) shows the interface bonding energy is essentially zero at approximately 0.4 nm, implying that the interaction between the two parts is small and a layered structure starts to form, consistent with the result shown in Fig. 8(b).

IV. CONCLUSION

Supertetragonal PbTiO_3 has made it necessary to revisit the linear relation, which is often implicitly assumed, between the polarization and the structural information. This work shows that the polarization-versus- c/a (or the relative ion displacement) curve demonstrates a sublinear increase at large axial ratio, which shall be taken into account to correctly interpret experimental results. We have found that the sublinear dependence can be ascribed to the decrease of the BECs with c/a . In addition, the relative displacement between cations, $\Delta_{\text{Ti-Pb}}$, behaves more like c/a than the polarization, making it an

improper measure of the polarization. Therefore, for the analysis based on HR(S)TEM images, it is critical to choose proper structural information from HR(S)TEM images (ideally the relative displacements between cations and anions, such as $\Delta_{\text{Ti-O}}$) to avoid quantitative inaccuracy or the sign problem as the polarization and the relative displacements between cations could be the same or totally opposite in direction, depending on the material under investigation.

ACKNOWLEDGMENTS

This work is financially supported by the National Natural Science Foundation of China (Grants No. 11974268 and No. 12111530061) and the Fundamental Research Funds for the Central Universities (FRF-MP-20-27). We acknowledge the support from the high-performance computing platform of Xi'an Jiaotong University.

- [1] P. Muralt, Ferroelectric thin films for micro-sensors and actuators: A review, *J. Micromech. Microeng.* **10**, 136 (2000).
- [2] H. S. Wang, S. K. Hong, J. H. Han, Y. H. Jung, H. K. Jeong, T. H. Im, C. K. Jeong, B. Y. Lee, G. Kim, C. D. Yoo, and K. J. Lee, Biomimetic and flexible piezoelectric mobile acoustic sensors with multiresonant ultrathin structures for machine learning biometrics, *Sci. Adv.* **7**, eabe5683 (2021).
- [3] G. Hodes, Perovskite-based solar cells, *Science* **342**, 317 (2013).
- [4] U.-G. Jong, C.-J. Yu, Y.-S. Kim, Y.-H. Kye, and C.-H. Kim, First-principles study on the electronic and optical properties of inorganic perovskite $\text{Rb}_{1-x}\text{Cs}_x\text{PbI}_3$ for solar cell applications, *Phys. Rev. B* **98**, 125116 (2018).
- [5] Y.-F. Ding, Z.-L. Yu, P.-B. He, Q. Wang, B. Liu, J.-L. Yang, and M.-Q. Cai, High-performance Photodetector Based on $\text{InSe}/\text{Cs}_2\text{XI}_2\text{Cl}_2$ ($X = \text{Pb}, \text{Sn}, \text{and Ge}$) Heterostructures, *Phys. Rev. Appl.* **13**, 064053 (2020).
- [6] Q. Mahmood, B. U. Haq, M. Yaseen, S. M. Ramay, M. G. B. Ashiq, and A. Mahmood, The first-principle study of mechanical, optical and thermoelectric properties of SnZrO_3 and SnHfO_3 for renewable energy applications, *Solid State Commun.* **292**, 17 (2019).
- [7] Y. M. Yaseen, H. Ambreen, R. Mehmood, M. Iqbal, J. Iqbal, T. Alshahrani, S. Noreen, and A. Laref, Investigation of optical and thermoelectric properties of PbTiO_3 under pressure, *Phys. B (Amsterdam, Neth.)* **615**, 412857 (2021).
- [8] B.-G. Kim, S. M. Cho, T.-Y. Kim, and H. M. Jang, Giant Dielectric Permittivity Observed in Pb-Based Perovskite Ferroelectrics, *Phys. Rev. Lett.* **86**, 3404 (2001).
- [9] Y. Fu and D. J. Singh, Thermal conductivity of perovskite KTaO_3 and PbTiO_3 from first principles, *Phys. Rev. Mater.* **2**, 094408 (2018).
- [10] J. F. Scott and C. A. Paz de Araujo, Ferroelectric memories, *Science* **246**, 1400 (1990).
- [11] M. Dawber, K. M. Rabe, and J. F. Scott, Physics of thin-film ferroelectric oxides, *Rev. Mod. Phys.* **77**, 1083 (2005).
- [12] J. F. Scott, Applications of modern ferroelectrics, *Science* **315**, 954 (2007).
- [13] A. F. Devonshire, XCVI. Theory of barium titanate, Part 1. *Philos. Mag.* **40**, 1040 (1949).
- [14] A. Amin, R. E. Newnham, and L. E. Cross, Atom shifts, polarization levels, and Curie temperatures in ferroelectric PbZrO_3 : PbTiO_3 solid solutions, *Mater. Res. Bull.* **15**, 721 (1980).
- [15] A. Amin, R. E. Newnham, and L. E. Cross, Phenomenological and structural study of a low-temperature phase transition in the PbZrO_3 - PbTiO_3 system, *J. Solid State Chem.* **37**, 248 (1981).
- [16] B. Jiang and L. A. Bursill, Phenomenological theory of size effects in ultrafine ferroelectric particles of lead titanate, *Phys. Rev. B* **60**, 9978 (1999).
- [17] C. Ederer and N. A. Spaldin, Effect of Epitaxial Strain on the Spontaneous Polarization of Thin Film Ferroelectrics, *Phys. Rev. Lett.* **95**, 257601 (2005).
- [18] T. Qi, I. Grinberg, and A. M. Rappe, Correlations between tetragonality, polarization, and ionic displacement in PbTiO_3 -derived ferroelectric perovskite solid solutions, *Phys. Rev. B* **82**, 134113 (2010).
- [19] Y. Ehara, S. Utsugi, M. Nakajima, T. Yamada, T. Iijima, H. Taniguchi, M. Itoh, and H. Funakubo, Spontaneous polarization estimation from the soft mode in strain-free epitaxial polar axis-oriented $\text{Pb}(\text{Zr}, \text{Ti})\text{O}_3$ thick films with tetragonal symmetry, *Appl. Phys. Lett.* **98**, 141914 (2011).
- [20] B. E. Warren, X-Ray diffraction in random layer lattices, *Phys. Rev.* **59**, 693 (1941).
- [21] W. M. Shume, H. C. Murthy, and E. A. Zereffa, A review on synthesis and characterization of Ag_2O nanoparticles for photocatalytic applications, *J. Chem.* **2020**, 9479 (2020).
- [22] L. Yao, P. Zou, L. Su, Y. Wu, Y. Pan, R. Fu, H. Min, L. Zhong, H. L. Xin, L. Sun, and F. Xu, In-situ TEM revisiting $\text{NH}_4\text{V}_4\text{O}_{10}$ to unveil the unknown sodium storage mechanism as an anode material, *Nano Energy* **87**, 106182 (2021).
- [23] C.-L. Jia, S.-B. Mi, K. Urban, I. Vrejoiu, M. Alexe, and D. Hesse, Effect of a Single Dislocation in a Heterostructure Layer on the Local Polarization of a Ferroelectric Layer, *Phys. Rev. Lett.* **102**, 117601 (2009).
- [24] C.-L. Jia, K. Urban, M. Alexe, D. Hesse, and I. Vrejoiu, Direct observation of continuous electric dipole rotation in flux-closure domains in ferroelectric $\text{Pb}(\text{Zr}, \text{Ti})\text{O}_3$, *Science* **331**, 1420 (2011).
- [25] L. Lu, Y. Dai, H. Du, M. Liu, J. Wu, Y. Zhang, Z. Liang, S. Raza, D. Wang, and C.-L. Jia, Atomic scale understanding of the epitaxy of perovskite oxides on flexible mica substrate, *Adv. Mater. Interfaces* **7**, 1901265 (2020).
- [26] D. Wang, Z. Fan, G. Rao, G. Wang, Y. Liu, C. Yuan, T. Ma, D. Li, X. Tan, Z. Lu, A. Feteira, S. Liu, C. Zhou, and S. Zhang, Ultrahigh piezoelectricity in lead-free piezoceramics by synergistic design, *Nano Energy* **76**, 104944 (2020).
- [27] Y. Dai, Z. Zhang, L. Lu, F. Zhang, L. Jin, D. Wang, Z. Li, and C.-L. Jia, Atomic-scale understanding of enhanced polarization of highly strained nanoscale columnar PbTiO_3 , *Phys. Rev. B* **104**, 184111 (2021).
- [28] S. C. Abrahams, S. K. Kurtz, and P. B. Jamieson, Atomic displacement relationship to curie temperature and spontaneous polarization in displacive ferroelectrics, *Phys. Rev.* **172**, 551 (1968).
- [29] C.-L. Jia, M. Lentzen, and K. Urban, Atomic-resolution imaging of oxygen in perovskite ceramics, *Science* **299**, 870 (2003).
- [30] K. Urban, Studying atomic structures by aberration-corrected transmission electron microscopy, *Science* **321**, 506 (2008).

- [31] C.-L. Jia, S.-B. Mi, J. Barthel, D. Wang, R. E. Dunin-Borkowski, K. Urban, and A. Thust, Determination of the 3D shape of a nanoscale crystal with atomic resolution from a single image, *Nat. Mater.* **13**, 1044 (2014).
- [32] H. Nan, J. Lu, M. Liu, H. Jing, S. Tang, D. Wang, and C.-L. Jia, Automatic and accurate determination of atom peak location in high-resolution electron microscopy image and fast visualization of polarization domains, *J. Chin. Electr. Microsc. Soc.* **35**, 191 (2016).
- [33] P. Zhao, H. Wang, L. Wu, L. Chen, Z. Cai, L. Li, and X. Wang, High-performance relaxor ferroelectric materials for energy storage applications, *Adv. Energy Mater.* **9**, 1803048 (2019).
- [34] Z. Sun, Z. Wang, Y. Tian, G. Wang, W. Wang, M. Yang, X. Wang, F. Zhang, and Y. Pu, Progress, outlook, and challenges in lead-free energy-storage ferroelectrics, *Adv. Electron. Mater.* **6**, 1900698 (2020).
- [35] G. Dong, S. Li, M. Yao, Z. Zhou, Y.-Q. Zhang, X. Han, Z. Luo, J. Yao, B. Peng, Z. Hu, H. Huang, T. Jia, J. Li, W. Ren, Z.-G. Ye, X. Ding, J. Sun, C.-W. Nan, L.-Q. Chen, J. Li *et al.*, Superelastic ferroelectric single-crystal membrane with continuous electric dipole rotation, *Science* **366**, 475 (2019).
- [36] E. Okunishi, H. Sawada, and Y. Kondo, Experimental study of annular bright field (ABF) imaging using aberration-corrected scanning transmission electron microscopy (STEM), *Micron* **43**, 538 (2012).
- [37] A. R. Damodaran, J. C. Agar, S. Pandya, Z. H. Chen, L. R. Dedon, R. Xu, B. A. Apgar, S. Saremi, and L. W. Martin, New modalities of strain-control of ferroelectric thin films, *J. Phys.: Condens. Matter* **28**, 263001 (2016).
- [38] J. L. MacManus-Driscoll, P. Zerrer, H. Wang, H. Yang, J. Yoon, A. Fouchet, R. Yu, M. G. Blamire, and Q. Jia, Strain control and spontaneous phase ordering in vertical nanocomposite heteroepitaxial thin films, *Nat. Mater.* **7**, 314 (2008).
- [39] L. Zhang, J. Chen, L. Fan, O. Diéguez, J. Cao, Z. Pan, Y. Wang, J. Wang, M. Kim, S. Deng, J. Wang, H. Wang, J. Deng, R. Yu, J. F. Scott, and X. Xing, Giant polarization in super-tetragonal thin films through interphase strain, *Science* **361**, 494 (2018).
- [40] Z. Zhang, Y. Dai, Z. Li, L. Lu, X. Zhang, K. Fu, X. Xu, W. Tian, C.-L. Jia, and Y. Jiang, Growth modulation of super-tetragonal PbTiO₃ thin films with self-assembled nanocolumn structures, *Adv. Electron. Mater.* **7**, 2100547 (2021).
- [41] B. A. Tuttle, D. A. Payne, and J. L. Mukherjee, Ferroelectric materials for dielectric power conversion, *Ferroelectrics* **27**, 219 (1980).
- [42] H. E. H. Ali, J. Ricote, M. L. Calzada, I. Bretos, and R. Jiménez, The influence of the crystallization temperature on the reliability of PbTiO₃ thin films prepared by chemical solution deposition, *J. Eur. Ceram. Soc.* **37**, 1449 (2017).
- [43] K. Iijima, Y. Tomita, R. Takayama, and I. Ueda, Preparation of *c*-axis oriented PbTiO₃ thin films and their crystallographic, dielectric, and pyroelectric properties, *J. Appl. Phys.* **60**, 361 (1986).
- [44] G. W. Berkstresser, A. J. Valentino, and C. D. Brandle, Congruent composition for growth of lanthanum aluminate, *J. Cryst. Growth* **128**, 684 (1993).
- [45] B. C. Chakoumakos, D. G. Schlom, M. Urbanik, and J. Luine, Thermal expansion of LaAlO₃ and (La, Sr)(Al, Ta)O₃, substrate materials for superconducting thin-film device applications, *J. Appl. Phys.* **83**, 1979 (1998).
- [46] P. D. Nellist, M. F. Chisholm, A. R. Lupini, A. Borisevich, W. H. Sides, Jr., S. J. Pennycook, N. Dellby, R. Keyse, O. L. Krivanek, M. F. Murfitt, and Z. S. Szilagy, Aberration-corrected STEM: Current performance and future directions, *J. Phys.: Conf. Ser.* **26**, 002 (2006).
- [47] S. J. Pennycook and D. E. Jesson, High-resolution Z-contrast imaging of crystals, *Ultramicroscopy* **37**, 14 (1991).
- [48] S. J. Pennycook, A. R. Lupini, M. Varela, A. Borisevich, Y. Peng, M. F. Chisholm, N. Dellby, O. L. Krivanek, P. D. Nellist, S. Z. Szilagy, and G. Duscher, Sub-Ångstrom resolution through aberration-corrected STEM, *Microsc. Microanal.* **9**, 926 (2003).
- [49] N. Shibata, A. Goto, K. Matsunaga, T. Mizoguchi, S. D. Findlay, T. Yamamoto, and Y. Ikuhara, Interface Structures of Gold Nanoparticles on TiO₂ (110), *Phys. Rev. Lett.* **102**, 136105 (2009).
- [50] Y. Kotaka, Essential experimental parameters for quantitative structure analysis using spherical aberration-corrected HAADF-STEM, *Ultramicroscopy* **110**, 555 (2010).
- [51] S. J. Pennycook, Z-contrast stem for materials science, *Ultramicroscopy* **30**, 58 (1989).
- [52] K. Urban, C.-L. Jia, L. Houben, M. Lentzen, S.-B. Mi, and K. Tillmann, Negative spherical aberration ultrahigh-resolution imaging in corrected transmission electron microscopy, *Philos. Trans. R. Soc. A* **367**, 3735 (2009).
- [53] C.-L. Jia, S.-B. Mi, K. Urban, I. Vrejoiu, M. Alexe, and D. Hesse, Atomic-scale study of electric dipoles near charged and uncharged domain walls in ferroelectric films, *Nat. Mater.* **7**, 57 (2008).
- [54] W. Zhong, R. D. King-Smith, and D. Vanderbilt, Giant LO-TO Splittings in Perovskite Ferroelectrics, *Phys. Rev. Lett.* **72**, 3618 (1994).
- [55] R. J. Zeches, M. D. Rossell, J. X. Zhang, A. J. Hatt, Q. He, C.-H. Yang, A. Kumar, C. H. Wang, A. Melville, C. Adamo, G. Sheng, Y.-H. Chu, J. F. Ihlefeld, R. Erni, C. Ederer, V. Gopalan, L. Q. Chen, D. G. Schlom, N. A. Spaldin, L. W. Martin *et al.*, A strain-driven morphotropic phase boundary in BiFeO₃, *Science* **326**, 977 (2009).
- [56] H. Béa, B. Dupé, S. Fusil, R. Mattana, E. Jacquet, B. Warot-Fonrose, F. Wilhelm, A. Rogalev, S. Petit, V. Cros, A. Anane, F. Petroff, K. Bouzouane, G. Geneste, B. Dkhil, S. Lisenkov, I. Ponomareva, L. Bellaiche, M. Bibes, and A. Barthélémy, Evidence for Room-Temperature Multiferroicity in a Compound with a Giant Axial Ratio, *Phys. Rev. Lett.* **102**, 217603 (2009).
- [57] J. X. Zhang, Q. He, M. Trassin, W. Luo, D. Yi, M. D. Rossell, P. Yu, L. You, C. H. Wang, C. Y. Kuo, J. T. Heron, Z. Hu, R. J. Zeches, H. J. Lin, A. Tanaka, C. T. Chen, L. H. Tjeng, Y.-H. Chu, and R. Ramesh, Microscopic Origin of the Giant Ferroelectric Polarization in Tetragonal-like BiFeO₃, *Phys. Rev. Lett.* **107**, 147602 (2011).
- [58] K. Carl, Ferroelectric properties and fatiguing effects of modified PbTiO₃ ceramics, *Ferroelectrics* **9**, 23 (1975).
- [59] H. Sharma, J. Kreisel, and P. Ghosez, First-principles study of PbTiO₃ under uniaxial strains and stresses, *Phys. Rev. B* **90**, 214102 (2014).

- [60] S. Tinte, K. M. Rabe, and D. Vanderbilt, Anomalous enhancement of tetragonality in PbTiO_3 induced by negative pressure, *Phys. Rev. B* **68**, 144105 (2003).
- [61] H. W. Shin and J. Y. Son, Tetragonally strained crystal structure and ferroelectric properties of epitaxial PbTiO_3 thin films grown on single-crystal Rh substrates, *Mater. Chem. Phys.* **264**, 124477 (2021).
- [62] S. Zhang, Y. Zhu, Y. Tang, Y. Liu, S. Li, M. Han, J. Ma, B. Wu, Z. Chen, S. Saremi, and X. Ma, Giant polarization sustainability in ultrathin ferroelectric films stabilized by charge transfer, *Adv. Mater.* **29**, 1703543 (2017).
- [63] J. Enkovaara, C. Rostgaard, J. J. Mortensen, J. Chen, M. Duřak, L. Ferrighi, J. Gavnholt, C. Glinsvad, V. Haikola, H. A. Hansen, H. H. Kristoffersen, M. Kuisma, A. H. Larsen, L. Lehtovaara, M. Ljungberg, O. Lopez-Acevedo, P. G. Moses, J. Ojanen, T. Olsen, V. Petzold *et al.*, Electronic structure calculations with GPAW: A real-space implementation of the projector augmented-wave method, *J. Phys.: Condens. Matter* **22**, 253202 (2010).
- [64] X. Gonze, J.-M. Beuken, R. Caracas, F. Detraux, M. Fuchs, G.-M. Rignanese, L. Sindic, M. Verstraete, G. Zerah, F. Jollet, M. Torrent, A. Roy, M. Mikami, Ph. Ghosez, J.-Y. Raty, and D. C. Allan, First-principles computation of material properties: The ABINIT software project, *Comput. Mater. Sci.* **25**, 478 (2002).
- [65] J. P. Perdew, K. Burke, and M. Ernzerhof, Generalized Gradient Approximation Made Simple, *Phys. Rev. Lett.* **77**, 3865 (1996).
- [66] R. D. King-Smith and D. Vanderbilt, Theory of polarization of crystalline solids, *Phys. Rev. B* **47**, 1651 (1993).
- [67] R. Resta, M. Posternak, and A. Baldereschi, Towards a Quantum Theory of Polarization in Ferroelectrics: The Case of KNbO_3 , *Phys. Rev. Lett.* **70**, 1010 (1993).
- [68] L. Lu, Y. Nahas, M. Liu, H. Du, Z. Jiang, S. Ren, D. Wang, L. Jin, S. Prokhorenko, C.-L. Jia, and L. Bellaiche, Topological Defects with Distinct Dipole Configurations in $\text{PbTiO}_3/\text{SrTiO}_3$ Multilayer Films, *Phys. Rev. Lett.* **120**, 177601 (2018).
- [69] Q. Yang, J. Cao, Y. Ma, and Y. Zhou, First principles study of polarization-strain coupling in $\text{SrBi}_2\text{Ta}_2\text{O}_9$, *AIP Adv.* **3**, 052134 (2013).
- [70] L. Patra and P. Ravindran, Magnetoelectric properties of Pb free $\text{Bi}_2\text{FeTiO}_6$: A theoretical investigation, in *2nd International Conference on Condensed Matter and Applied Physics (ICC 2017)*, edited by M. S. Shekhawat, S. Bhardwaj, and B. Suthar, AIP Conf. Proc. No. 1953 (AIP, New York, 2018), p. 120039.
- [71] C. Li, S. Zheng, H. Wang, J. Gong, X. Li, Y. Zhang, K. Yang, L. Lin, Z. Yan, S. Dong, and J.-M. Liu, Structural transitions in hybrid improper ferroelectric $\text{Ca}_3\text{Ti}_2\text{O}_7$ tuned by site-selective isovalent substitutions: A first-principles study, *Phys. Rev. B* **97**, 184105 (2018).
- [72] Y. Zhang, J. Sun, J. P. Perdew, and X. Wu, Comparative first-principles studies of prototypical ferroelectric materials by LDA, GGA, and SCAN meta-GGA, *Phys. Rev. B* **96**, 035143 (2017).
- [73] V. R. Cooper and K. M. Rabe, Enhancing piezoelectricity through polarization-strain coupling in ferroelectric superlattices, *Phys. Rev. B* **79**, 180101(R) (2009).
- [74] S. P. Beckman, X. Wang, K. M. Rabe, and D. Vanderbilt, Ideal barriers to polarization reversal and domain-wall motion in strained ferroelectric thin films, *Phys. Rev. B* **79**, 144124 (2009).
- [75] M. J. Haun, E. Furman, S. J. Jang, H. A. McKinstry, and L. E. Cross, Thermodynamic theory of PbTiO_3 , *J. Appl. Phys.* **62**, 3331 (1987).
- [76] N. A. Pertsev, A. G. Zembilgotov, and A. K. Tagantsev, Effect of Mechanical Boundary Conditions on Phase Diagrams of Epitaxial Ferroelectric Thin Films, *Phys. Rev. Lett.* **80**, 1988 (1998).
- [77] D. D. Fong, C. Cionca, Y. Yacoby, G. B. Stephenson, J. A. Eastman, P. H. Fuoss, S. K. Streiffer, C. Thompson, R. Clarke, R. Pindak, and E. A. Stern, Direct structural determination in ultrathin ferroelectric films by analysis of synchrotron x-ray scattering measurements, *Phys. Rev. B* **71**, 144112 (2005).
- [78] P. Ghosez, J.-P. Michenaud, and X. Gonze, Dynamical atomic charges: The case of ABO_3 compounds, *Phys. Rev. B* **58**, 6224 (1998).
- [79] Y.-X. Wang, Giant static dielectric constant of strained PbTiO_3 , *Chin. Phys. Lett.* **26**, 016801 (2009).
- [80] Y. Duan, L. Qin, G. Tang, and C. Chen, Effect of epitaxial strain on the properties of short-period $\text{BaTiO}_3/\text{PbTiO}_3$ superlattice from first-principles calculations, *Phys. Lett. A* **374**, 2075 (2010).
- [81] Z. Jiang, R. Zhang, F. Li, L. Jin, N. Zhang, D. Wang, and C.-L. Jia, Electrostriction coefficient of ferroelectric materials from *ab initio* computation, *AIP Adv.* **6**, 065122 (2016).
- [82] G. Shirane and S. Hoshino, On the phase transition in lead titanate, *J. Phys. Soc. Jpn.* **6**, 265 (1951).
- [83] Y. L. Tang, Y. L. Zhu, X. L. Ma, A. Y. Borisevich, A. N. Morozovska, E. A. Eliseev, W. Y. Wang, Y. J. Wang, Y. B. Xu, Z. D. Zhang, and S. J. Pennycook, Observation of a periodic array of flux-closure quadrants in strained ferroelectric PbTiO_3 films, *Science* **348**, 547 (2015).
- [84] C.-L. Jia, L. Jin, D. Wang, S.-B. Mi, M. Alexe, D. Hesse, H. Reichlova, X. Marti, L. Bellaichef, and K. Urbana, Nanodomains and nanometer-scale disorder in multiferroic bismuth ferrite single crystals, *Acta Mater.* **82**, 356 (2015).
- [85] A. M. Glazer, S. A. Mabud, and R. Clarke, Powder profile refinement of lead zirconate titanate at several temperatures. II. Pure PbTiO_3 , *Acta Cryst.* **34**, 1065 (1978).